\$ 50 CONTRACTOR OF THE SECOND SECOND

Contents lists available at ScienceDirect

Chaos, Solitons and Fractals

journal homepage: www.elsevier.com/locate/chaos



Extended networks as a route of stabilization of divergent dynamics

Vagner dos Santos ^a, Matheus Rolim Sales ^b, Iberê Luiz Caldas ^b, Ricardo Luiz Viana ^d, José Danilo Szezech Jr. ^{c,f,g},

- ^a Department of Physics, State University of Ponta Grossa, 84030-900, Ponta Grossa, PR, Brazil
- ^b São Paulo State University (UNESP), Institute of Geosciences and Exact Sciences, 13506-900, Rio Claro, SP, Brazil
- ^c Institute of Physics, University of São Paulo, 05315-970, São Paulo, SP, Brazil
- ^d Department of Physics, Federal University of Paraná, 81531-980, Curitiba, PR, Brazil
- e Centro Interdisciplinar de Ciência, Tecnologia e Inovação, Núcleo de Modelagem e Computação Científica, 81531-980, Curitiba, PR, Brazil
- f Graduate Program in Sciences/Physics, State University of Ponta Grossa, 84030-900, Ponta Grossa, PR, Brazil
- g Department of Mathematics and Statistics, State University of Ponta Grossa, 84030-900, Ponta Grossa, PR, Brazil

ARTICLE INFO

Keywords: Nonlinear dynamics Coupled Hénon maps Coherent and incoherent spatial states

ABSTRACT

This work examines the dynamical states of coupled Hénon maps that arise due to the network's coupling configuration in a ring topology. The parameters for each individual node are selected in a way that ensures the absence of stable attractors in phase space, such that in the event of synchronization across the network, all maps exhibit divergence after a brief transient period. However, contrary to what one would expect, we find that the coupled network demonstrates the ability to stabilize and produce non-divergent dynamics, depending on the coupling strength and radius. Thus, the dynamical states observed following the transient phase are exclusively a consequence of the network's coupling. Using spatial recurrence matrix, the study correlates nondivergent dynamics with parameter regions prone to chimera and incoherent states, demonstrating multistability for certain coupling strengths and showing that individual nodes' dynamics remain close to the chaotic saddle of the uncoupled maps. The paper is organized to discuss the Hénon map, coupling mechanisms, characterization of nondivergent states and dynamical switch states transitions.

1. Introduction

Networks are present in both physical and abstract realms, connecting everything from electrical grids to social relationships and biological systems [1]. Networks of coupled maps, for instance, are a widely studied type of spatially extended systems, characterized by discrete space and time variables with continuous state variables [2,3]. These systems consist of local dynamical units that interact with each other through a coupling structure in a complex topology. They have been used in mathematical models to explore various phenomena, including secure communication [4], image encryption [5], biological neuronal networks [6–9] and spatiotemporal chaos [10]. In recent years, it has become of great interest the understanding of the dynamics of systems coupled according to a complex network topology. The research in this area has found important phenomena such as cascade effects [11], synchronization patterns [12], and chimera states [13,14].

Chimera states have the peculiar characteristic of presenting simultaneously coherent and incoherent behaviors in a network. This curious phenomenon was first reported by Kuramoto and Battogtokh in 2002 [13], where under suitable conditions, peculiar patterns emerged

in coupled phase oscillators. The combination of coherent and incoherent states was named chimera states [14], referring to a creature in Greek mythology composed of distinct animals. An interesting review of chimera states applied in neuronal networks is presented in [15, 16]. Experiments with coupled mechanical oscillators are discussed in [17,18], and chimera states in populations of nonlocally coupled chemical oscillators are examined in [19,20]. Reports of the presence of chimera states in SQUID metamaterial [21,22] indicate possible application of this dynamical behavior. Another potential application of coexistent states is the unihemispheric sleep in some aquatic mammals and birds, where one cerebral hemisphere sleeps while the other remains awake [23,24], as well as the similarities between the collapses of chimera states and epileptic seizures, as pointed out by Andrzejak et al. [25].

It has been shown that the chaotic saddle plays a role in the long-term dynamics of networks of coupled maps, trapping trajectories for times that may be arbitrarily long [26,27]. In this paper, we investigate the dynamics of a network of coupled Hénon maps in a ring topology. For the set of parameters used, the uncoupled Hénon map exhibits no

^{*} Corresponding author at: Department of Mathematics and Statistics, State University of Ponta Grossa, 84030-900, Ponta Grossa, PR, Brazil. *E-mail address:* jdsjunior@uepg.br (J.D. Szezech Jr.).

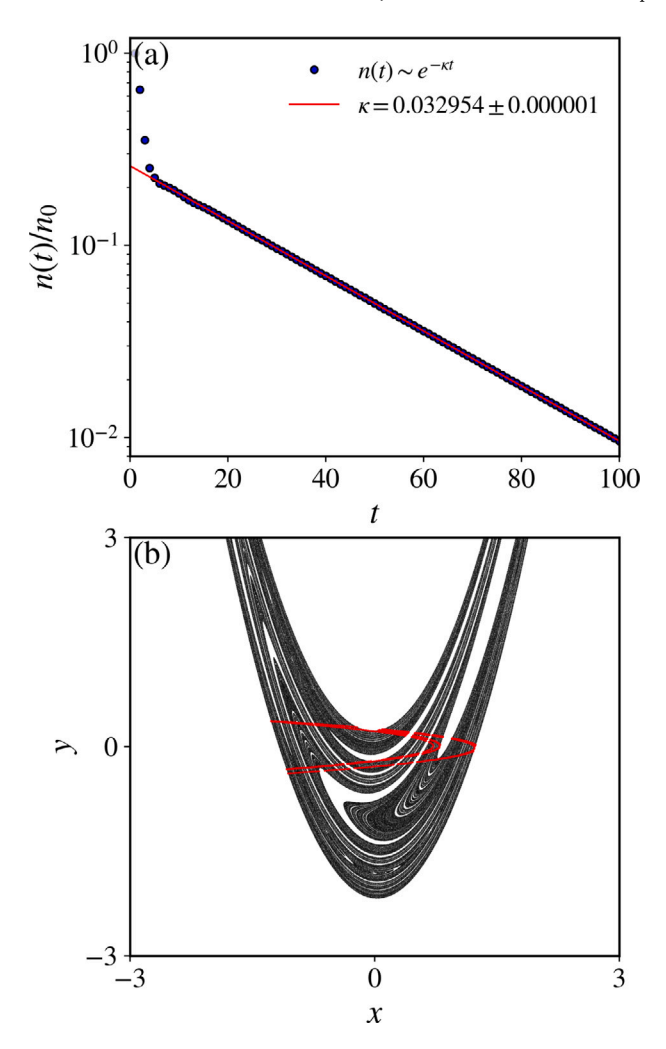


Fig. 1. (a) The fraction of nondivergent initial conditions as a function of time for the uncoupled Hénon map. We consider $n_0=10^8$ initial conditions uniformly distributed in a $10^4\times10^4$ grid. (b) The chaotic saddle (red) and its stable manifold (black). The parameters used are $\alpha=1.5$ and $\beta=0.3$. (For interpretation of the references to color in this figure legend, the reader is referred to the web version of this article.)

stable attractors and is divergent. Nevertheless, the coupled network acts as a mechanism of stabilization and generation of nondivergent dynamics depending on the coupling strength and radius. By the characterization of the dynamic state using the method of spatial recurrence matrix [28,29] we were able to relate the nondivergent dynamics with the regions in parameter space more prone to the existence of chimera and incoherent states. Furthermore, we show the existence of multistability for some values of coupling strength and that the individual node dynamics remain close to the chaotic saddle present in the uncoupled maps phase space.

This paper is organized as follows. In Section 2, we introduce the Hénon map and discuss the coupling mechanisms and some properties of the divergent behavior for specific parameters. In Section 3, we describe the methodology to determine the different nondivergent states and their dependence on the strength and radius of the coupling. In Section 4, we analyze how the network can switch between dynamical states and the crises of stabilized states. At last, Section 5 contains our final remarks and conclusions.

2. Network model

In this paper, we investigate the dynamics of a network of N identical Hénon maps coupled in a ring topology. The dynamics of the

$$\begin{aligned} &\text{nodes is given by} \\ &x_{t+1}^{(i)} = F_x \bigg(x_t^{(i)}, y_t^{(i)} \bigg) \\ &+ \frac{\sigma}{2rN} \sum_{j=i-rN}^{i+rN} \bigg[F_x \bigg(x_t^{(j)}, y_t^{(j)} \bigg) - F_x \bigg(x_t^{(i)}, y_t^{(i)} \bigg) \bigg], \\ &y_{t+1}^{(i)} = F_y \bigg(x_t^{(i)}, y_t^{(i)} \bigg), \end{aligned}$$

where $i=1,2,\ldots,N$, t is the discrete-time, $(x_t^{(i)},y_t^{(i)})$ is the ith node state at time t, $F_x(x,y)=1-\alpha x^2+y$ and $F_y(x,y)=\beta x$ are the equations of the two-dimensional Hénon map, and σ and r are the coupling strength and coupling radius, respectively.

For parameters $\alpha=1.5$ and $\beta=0.3$, the uncoupled Hénon map exhibits a divergent behavior, in which a typical initial condition diverges towards infinity after a few iterations. However, due to the presence of a chaotic saddle, some initial conditions may remain a long transient time in a chaotic regime before escaping towards infinity [30]. We characterize such a chaotic saddle through the average decay time. We consider a number n_0 of initial conditions inside the interval $(x,y) \in [-3,3] \times [-3,3]$, and calculate the number of initial conditions, n(t), that remain inside the interval at time t. If there is a chaotic saddle in the interval, n(t) exhibits an exponential decay, $n(t) \sim e^{-\kappa t}$, where κ is the decay rate [Fig. 1(a)]. The average decay time is the reciprocal of κ , i.e., $\tau=1/\kappa$. The chaotic saddle (red) and its stable manifold (black) for the uncoupled Hénon map is shown in Fig. 1(b).

Next, we investigate the influence of the coupling on the dynamics using the same parameters we have used for the uncoupled case, *i.e.*, $\alpha=1.5$ and $\beta=0.3$. Due to the form of the coupling term in Eq. (1), if the nodes of the network are synchronized, then the coupling function will be zero and each map will behave as in the uncoupled case. As there are no stable attractors, the system will diverge. The consequence is that the only remaining dynamic states observed in the network will be due to the network coupling.

For the network, we select random initial conditions in the interval $(x, y) \in [-0.1, 0.1] \times [-0.1, 0.1]$ and following our previous analysis, we investigate the behavior of n(t) as a function of t and the coupling strength, σ , for distinct values of the coupling radius, r (Fig. 2), namely, (a) r = 0.05, (b) r = 0.10, (c) r = 0.15, (d) r = 0.20, (e) r = 0.25, (f) r = 0.30, (g) r = 0.35, (h) r = 0.40, (i) r = 0.45, and (j) r = 0.50.

Depending on the combination of σ and r, the network exhibits very different dynamics. For instance, for $\sigma \approx 0$, all initial conditions diverge, as expected, due to the weak coupling. For large values of σ and r, all initial conditions diverge as well. The interesting nontrivial dynamics occurs for intermediate values of σ and r. We notice that for all values of r and $\sigma \lesssim 0.38$, no initial conditions diverge (gray color) at least until t = 5000. However, it is observable from Fig. 2 that most of the color scales have a flat profile, so we do not expect any significant modifications for larger t. We also emphasize that we do not observe transients of chimera states or a collapse of such states, even for larger times. Our guess is that, despite the finite size of our network, the size N = 1000 in our simulations results in very long times or even infinity to reach collapses. This is in agreement with the results of Wolfrum and Omel'chenko [31], where for continuous-time systems, the average lifetimes of chimera states increase exponentially with the size of the network. As r increases and the network approaches global coupling (r = 0.5), about 10% of the initial conditions start to diverge (red color). On the other hand, for small values of r, a substantial number of initial conditions diverge for large σ while the remaining stay on the interval and n(t) reaches a constant value (up to 5000 iterations). Therefore, the dynamics is highly nontrivial on the parameters σ and r. In order to investigate which parameter set results in more nondivergent initial conditions, we calculate n(t) at t = 5000 in the parameter space $\sigma \times r$ (Fig. 3).

We observe a wide range of parameter values where no initial conditions diverge towards infinity (gray color). In contrast, there are regions where all initial conditions diverge. These regions are interspersed with

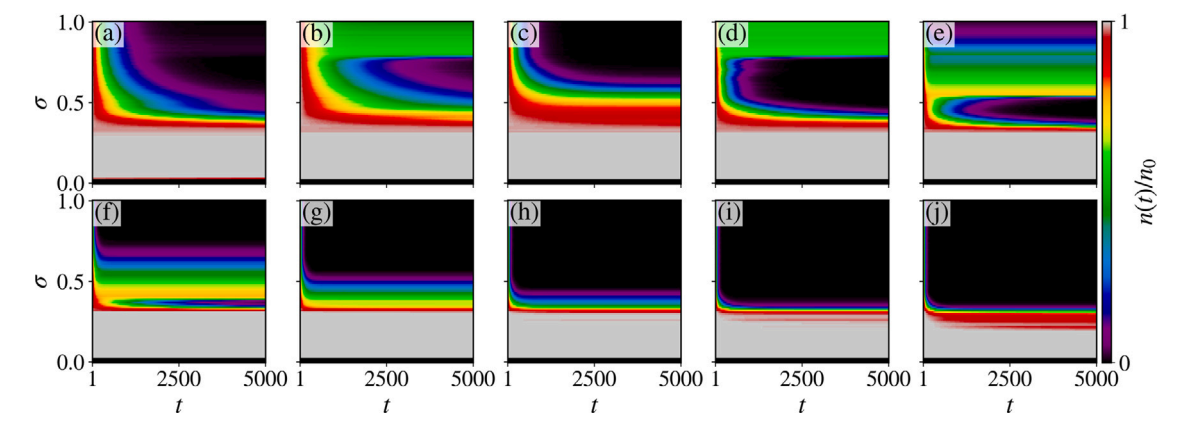


Fig. 2. The fraction $n(t)/n_0$ of nondivergent initial conditions as a function of time for the network, Eq. (1), for changing coupling strength σ with (a) r = 0.05, (b) r = 0.10, (c) r = 0.15, (d) r = 0.20, (e) r = 0.25, (f) r = 0.30, (g) r = 0.35, (h) r = 0.40, (i) r = 0.45, and (j) r = 0.50. The parameters used are N = 1000, $n_0 = 10^3$, $\alpha = 1.5$, and $\beta = 0.3$.

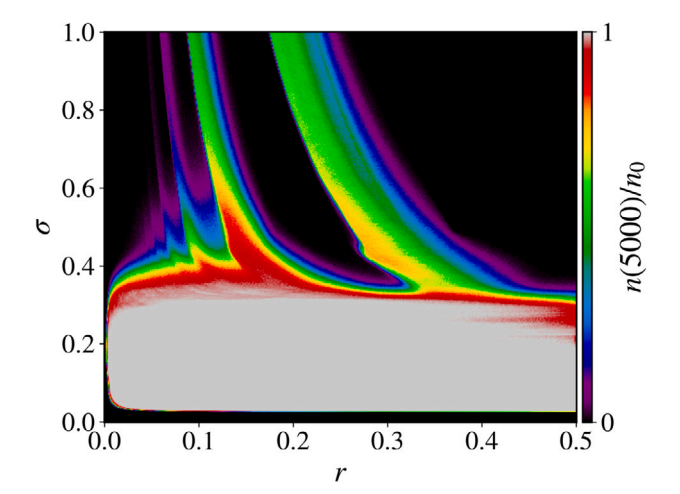


Fig. 3. The fraction of nondivergent initial conditions for the network, Eq. (1), at t=5000 for a grid of 500×500 values of (r,σ) . The parameters used are N=1000, $n_0=10^3$, $\alpha=1.5$, and $\beta=0.3$.

areas where only some initial conditions diverge. Hence, we observe a stabilization of the divergent dynamics of the uncoupled system due to the coupling. The top right corner of Fig. 3 is the region where usually takes place the synchronization of the network, with the bounds of the parameter values for synchronization being determined by the method of the master stability function [32]. However, in order to determine these parameter values it is necessary a trajectory in the synchronization manifold. This trajectory cannot be obtained for the parameters of the Hénon map used here, as there is no stable attractor and all trajectories are unbounded. Moreover, the diagram shown in Fig. 3 remarkably resembles diagrams with regions of coherence such as the one shown in Figure 1 of Ref. [33], for example. In our case, however, it remains unclear which configurations and dynamical states of the network correspond to each region in the diagram $\sigma \times r$. In Section 3, we present the extended version of spatial recurrence matrix to characterize the dynamical states of our network [28,29].

3. Characterization of the network dynamical states

A large variety of approaches already exist for the quantification of dynamical states, particularly with regard to chimera-like patterns. These approaches include the local order parameter [33–35], the strength of incoherence [36], the spatial inverse participation ratio [37], the normalized probability density function of the discrete Laplacian [38], among others. Specifically, Kemeth and collaborators

also proposed a scheme to classify chimera states [38]. As each approach has its strengths and weaknesses, our study uses an approach based on the binary distance matrix, introduced by Santos and collaborators [39] as a modification of the eigenvalue decomposition method [40]. The chosen method contrasts with those mentioned above, as it identifies coherent nodes that are not close neighbors and does not require the computation of eigenvalues and eigenvectors, thus reducing computation time.

Given the node's state variables time series $\mathbf{x}_t^{(i)} = (x_t^{(i)}, y_t^{(i)})^T$, we construct the symmetric spatial distance matrix \mathbf{d} according to

$$d_{ij} = \left\langle \left\| x_t^{(i)} - x_t^{(j)} \right\| \right\rangle_{\perp},\tag{2}$$

where $\|\cdot\|$ is the Euclidean norm, $\langle\cdot\rangle_t$ denotes the average in time, and $i,j=1,2,\ldots,N$. If nodes i and j are coherent with each other, $d_{ij}\approx 0$, and large values of d_{ij} indicate incoherence. By computing the binary distance matrix as

$$L_{ij} = H(d_{ij} - \varepsilon), \tag{3}$$

with $\varepsilon>0$ being a small threshold and $H(\cdot)$ is the Heaviside unit step function, we assign the value '1' for the coherent nodes and the value '0' for the incoherent ones. In other words, if the mean distance between $x^{(i)}$ and $x^{(j)}$ in some time interval is smaller than ε , L_{ij} equals 1 and zero otherwise. This particular definition of L_{ij} resembles the definition of the recurrence matrix used in recurrence quantification analysis (RQA) [41–46]. However, in RQA, the recurrence matrix is constructed using the time series of the state variables, whereas in our case, we compute L_{ij} using the state variables of the nodes in the network. Such a definition is often called spatial recurrence matrix [28,29].

For a completely incoherent state, the matrix \mathbf{L} takes on the form of the identity matrix. When there is coherence among certain nodes, specific off-diagonal elements of \mathbf{L} become non-zero, and when the state is entirely coherent, all elements of the matrix \mathbf{L} are one. Therefore, one can distinguish among these different states by applying the following methodology:

- 1. Sum the elements of each column of the matrix \mathbf{L} : $s_j = \sum_i L_{ij}$, for $i,j=1,2,\ldots,N$. If the jth node is incoherent with the rest of the network, then $s_j=1$, as all column elements are zero except for the diagonal element. If there is coherence with another node, then $s_j>1$.
- 2. Apply the sign function on the sum of each column as $S_i = \text{sign}(s_i 1)$. This function assigns the value 1 to the coherent nodes, as $s_i > 1$, and the value 0 for the incoherent ones.
- 3. Sum the elements of S: $C = \sum_i S_i$, where C = N represents cluster synchronization and C = 0 shows that all the nodes are desynchronized. A coherence–incoherence state, also called a chimera state, is characterized by intermediate values of C,

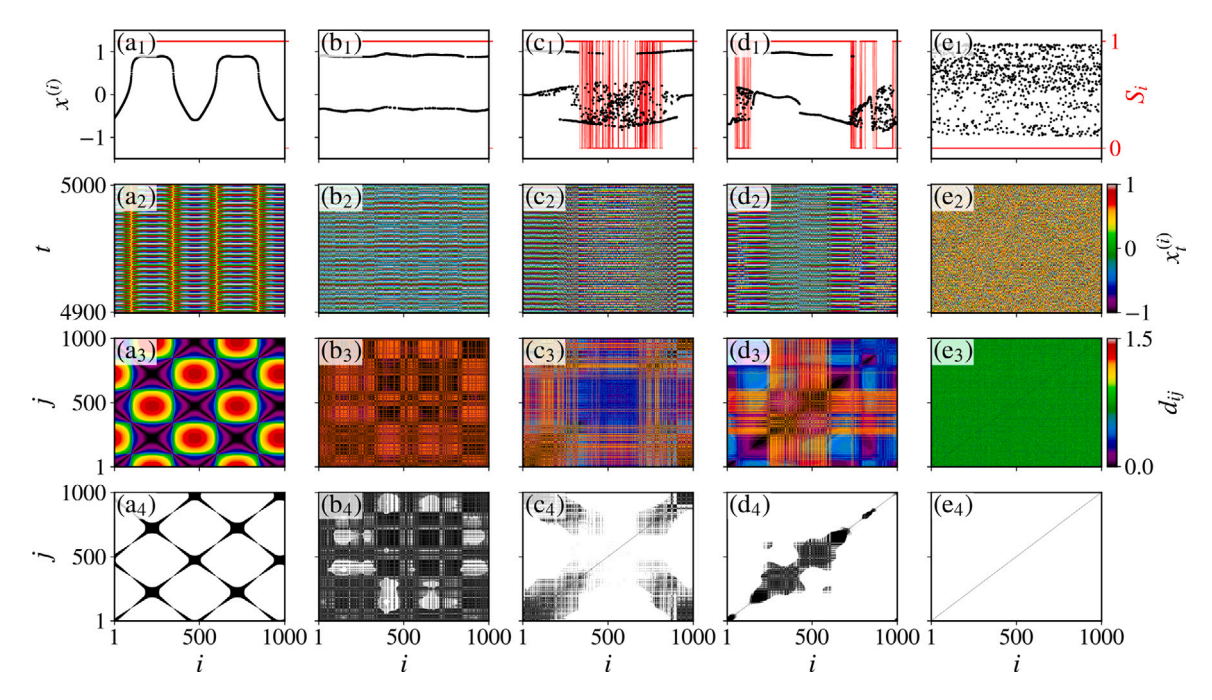


Fig. 4. (Black) The snapshot of $x_i^{(l)}$ at t = 5000 and (red) the vector S (1st row) and the spatio-temporal evolution of $x_i^{(l)}$ (2nd row) of Eq. (1), the distance matrix (3rd row), and the binary distance matrix (4th row) for (a) $(r, \sigma) = (0.15, 0.50)$, (b) $(r, \sigma) = (0.45, 0.25)$, (c) $(r, \sigma) = (0.30, 0.22)$, (d) $(r, \sigma) = (0.30, 0.25)$, and (e) $(r, \sigma) = (0.10, 0.10)$. The parameters used are N = 1000, ε = 7.5δ/100, where ε is the standard deviation defined in the main text, ε = 1.5, and ε = 0.3. The cases (a) and (b) shows examples of states with ε = 0. (For interpretation of the references to color in this figure legend, the reader is referred to the web version of this article.)

0 < C < N, i.e., C nodes belong to synchronized clusters and N - C nodes are desynchronized.

To obtain ${\bf L}$, it is necessary to define the threshold ε in (3). This parameter has to be chosen carefully as if ε is chosen too large, almost every node is coherent with every other node. On the other hand, if ε is chosen too small, this analysis will result in almost no coherent nodes in the network, even if they are indeed spatially coherent, and we can extract no information from ${\bf L}$. Therefore, the choice of ε has to be a compromise between having ε as small as possible and at the same time not too small so that there will be no coherent nodes. Regarding RQA, several rules of thumb have been proposed [47–49], but one of them is particularly interesting for taking into account the data dispersion: the threshold is considered to depend upon the standard deviation of the data series [44,50–52]. Here, we consider the standard deviation of the time series $x_t^{(i)}$ of each individual node, resulting in a standard deviation vector $\delta = (\delta_1, \delta_2, \ldots, \delta_N)$. We define the threshold to be 7.5% of the mean value of δ , i.e.,

$$\varepsilon = \frac{7.5}{100}\delta,\tag{4}$$

where $\delta = \frac{1}{N} \sum_{i=1}^{N} \delta_i$. For a discussion regarding the effect of the threshold ε on our results, see Appendix A.

We apply this methodology to the states shown in the first two rows of Fig. 4. The last two rows of Fig. 4 show the distance matrix **d** and the binary matrix **L**, respectively. For the first two states, (a) and (b), every node is coherent with at least one other node of the network. Hence $S_i = 1$ for all i = 1, 2, ..., N, C = N and we observe coherent states. For states (c) and (d), we identify several incoherent nodes coexisting with coherent ones. In these cases 0 < C < N holds as $S_i = 0$ for some nodes, and we observe coherence–incoherence states. The remaining state, (e), corresponds to an incoherent state, with $S_i = 0$ for all i and C = 0.

Therefore, using the proposed methodology, we can accurately characterize the dynamical states of our network. In order to analyze which configuration and state correspond to each region in the parameter space $\sigma \times r$, we divide this space into a 300 \times 300 grid, and for each pair (σ,r) , we consider $n_0=10^3$ initial conditions and apply the described methodology to each one of them. We plot the fraction of initial

conditions that converge to each state in Fig. 5. Note that Fig. 5(a) and Fig. 3 are the same, First, for values of σ above $\sigma_c \approx 0.53$, which marks the end of the incoherence–coherence transition, the initial conditions either diverge or correspond to coherent states. This σ_c was analytically determined for a network of identical coupled Hénon maps [53,54] as $\sigma_c = 1 - 1/|\beta + 2\alpha x^*|$, where x^* is the fixed point of the map. This value corresponds to the point where the smooth profile breaks up and the spatial derivative becomes infinite.

An exception exists in a small region in Fig. 5(c) near the line $\sigma=\sigma_c$ that our methodology identifies as coherence–incoherence states. This misidentification is due to numerical artifacts, such as the finite size of our network. Increasing the network size will eliminate these erroneous detections. However, these incorrectly identified states constitute only a small fraction of our total number of initial conditions and they do not influence our analysis. For $\sigma<\sigma_c$, the network exhibits all three nondivergent possible states, *i.e.*, coherence, coherence–incoherence and incoherence.

Therefore, different initial conditions exhibit very distinct dynamics and final states. Furthermore, even though the uncoupled dynamics is divergent, when we turn on the coupling, the dynamics stabilizes even for small coupling strength and radius. Additionally, divergent, coherent, and coherent–incoherent states coexist for the same parameter values, and, interestingly enough, divergent and incoherent states do not coexist. In Section 4 we analyze the transitions between these different dynamical states depending on the direction of the parameter change.

4. Hysteresis and multistability of the stabilized states

To analyze how the network switches its dynamical state among all possible states, we select a fixed random initial condition and fix the coupling radius as r=0.25. Next, we vary the coupling strength in the interval $\sigma \in [0.12, 0.30]$ in both directions following the dynamical state, i.e., for each new parameter value, the initial condition corresponds to the last state of the previous value of σ . We also calculate the final state for each σ value and plot the Single-node orbit diagram with colored

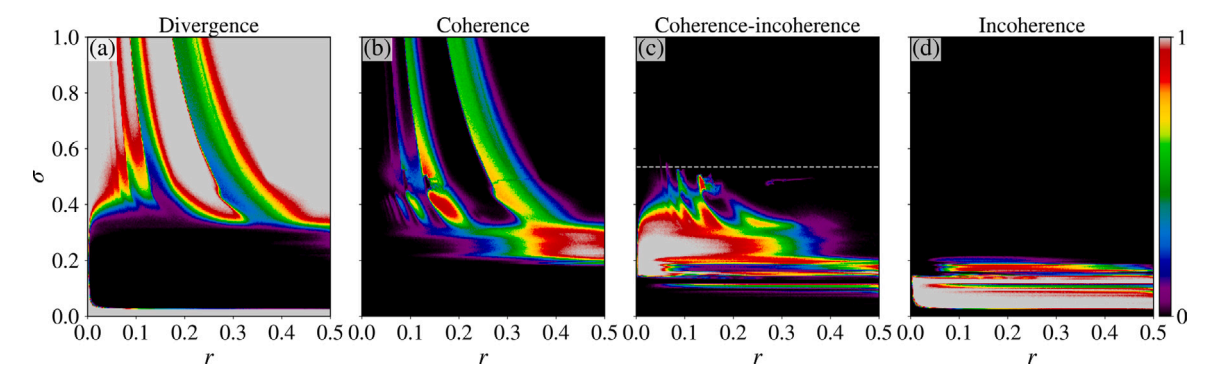


Fig. 5. Fraction of initial conditions that converges to each state in the parameter $\sigma \times r$ for the network, Eq. (1), with N=1000, $n_0=10^3$, $\alpha=1.5$, and $\beta=0.3$. The dashed white horizontal line in (c) corresponds to the transition value $\sigma_c=0.53$ that marks the coherence–incoherence transition. (For interpretation of the references to color in this figure legend, the reader is referred to the web version of this article.)

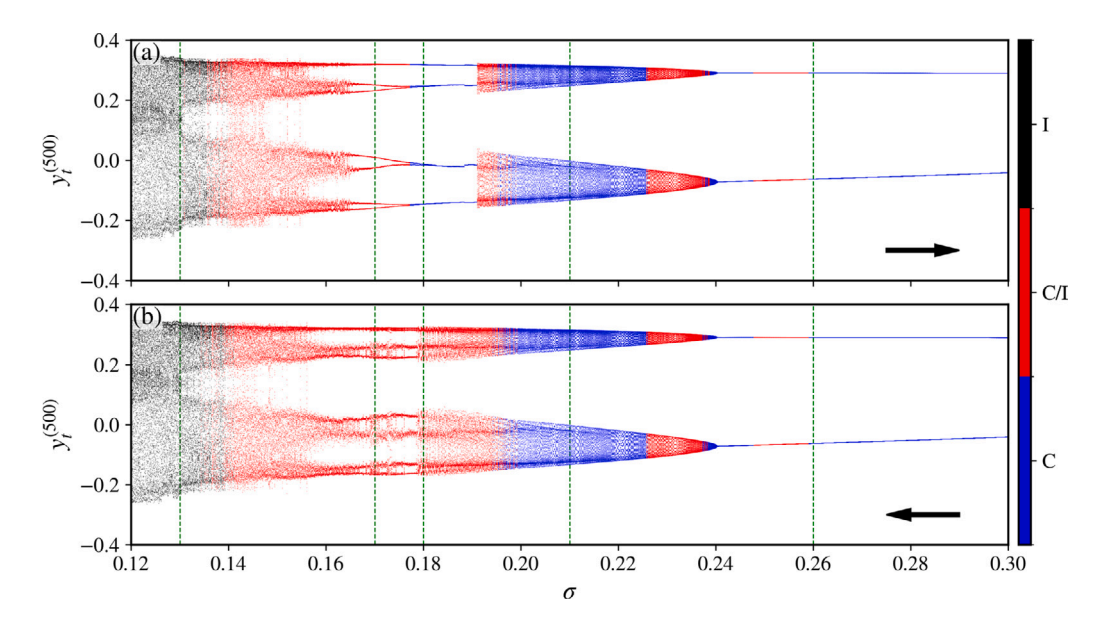


Fig. 6. Single-node orbit diagram with (a) increasing σ and (b) decreasing σ with r = 0.25, N = 1000, $\alpha = 1.5$, and $\beta = 0.3$. We plot the y variable of the 500th node and we color the point according to the state of the network. For a completely coherent (incoherent) state, we color the point blue (black). When coherent and incoherent nodes coexist, we color the point red. The green dashed vertical lines correspond to the values of σ we plot the phase space of the network (Fig. 7). (For interpretation of the references to color in this figure legend, the reader is referred to the web version of this article.)

points (Fig. 6). For a completely coherent (incoherent) state, we color the point blue (black). If coherent and incoherent nodes coexist, we color the point red.

In Fig. 6(a) we observe the dynamical behavior of node i=500 when the coupling parameter increases, and in Fig. 6(b) when the coupling parameter decreases. It must be noted that this is not a single-node orbit diagram in the classical sense of dynamical systems, i.e. for $\sigma=0.175$ it could be wrongly concluded that the system is in a periodic orbit of period 8, however, we are only seeing one node of the network, while other parts of the network, in the incoherent region, present nonperiodic dynamics and is marked with red (coherent and incoherent coexistence). Comparing Figs. 6(a) and (b) we can clearly see the existence of multistability in the network so that the final dynamical state is different whether the σ parameter is increasing or decreasing.

The five green dashed vertical lines in Fig. 6 correspond to the values of σ for which we plot the "phase space" of the network (Fig. 7), *i.e.*, we plot the values of x and y for all nodes of the network and we color the point blue (red) if the node is coherent (incoherent). In Fig. 7(a) both the states are completely incoherent (red). For a larger value of σ [Fig. 7(b)], both states exhibit coherent and incoherent nodes (blue and red). For the cases in Figs. 7(c) and 7(d), the state obtained increasing σ is a completely coherent state (blue), whereas the state obtained decreasing σ exhibits both coherent and incoherent

nodes (blue and red). Finally, the states in Fig. 7(e) correspond to the same dynamical state, *i.e.*, completely coherent (blue), however with two distinct attractors positions. To analyze how the nodes are distributed in phase space, we divide it in a grid of 1000×1000 boxes and we count the number of times a box has been occupied. In Fig. 8 we plot the phase space and the occupancy for $\sigma=0.174$ obtained by varying σ in both directions. We notice regions with larger occupancy [green to red color in Figs. 8(b) and 8(d)] and these regions correspond to the location of the coherent nodes [blue points in Figs. 8(a) and 8(c)]. We also plot the phase space and the occupancy for values of σ varying in the interval $\sigma \in [0.12, 0.30]$ in both directions (ascending and descending order) in Supplementary Videos forward.avi and backward.avi. This clustering of nodes in specific regions in phase space repeats for all values of σ that exhibit coherent nodes.

5. Conclusions

In this paper, we have analyzed the dynamics of a network of N identical Hénon maps coupled in a ring topology. The uncoupled Hénon map is known to exhibit divergent behavior for specific parameter values and we have chosen our set of parameters in such a way that the uncoupled case is divergent. We have found that depending on the value of the coupling strength σ and the coupling radius r, the network

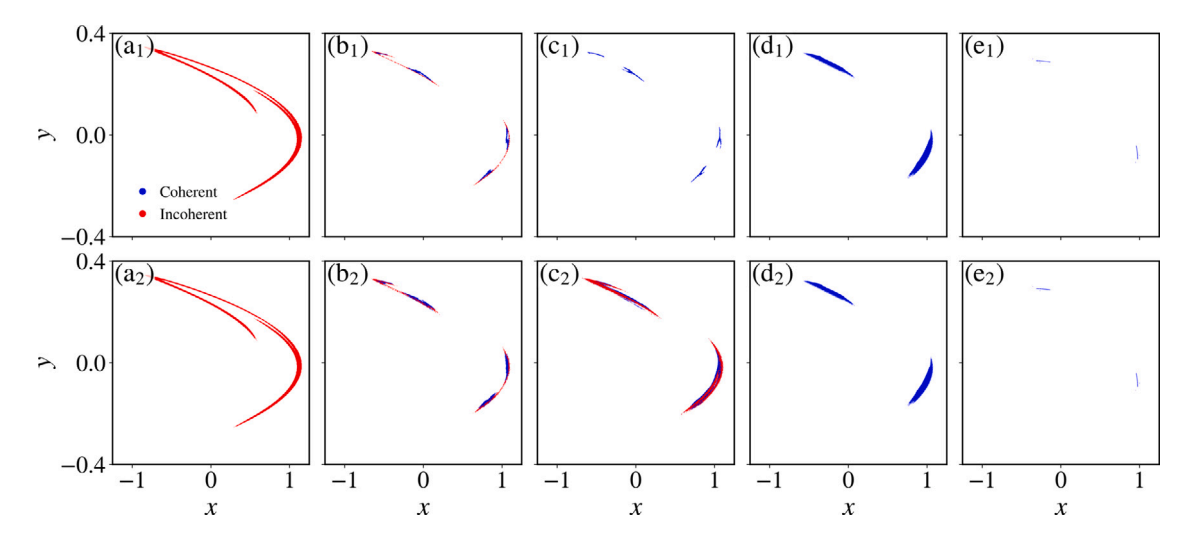


Fig. 7. The phase space of the network for different values of σ with (top row) increasing σ and (bottom row) decreasing σ . We plot the x and y positions of each node after the transient and we color in blue (red) the coherent (incoherent) nodes. The green dashed vertical lines in Fig. 6 correspond to the values of σ , namely, (a) $\sigma = 0.13$, (b) $\sigma = 0.17$, (c) $\sigma = 0.18$, (d) $\sigma = 0.21$, and (e) $\sigma = 0.26$. (For interpretation of the references to color in this figure legend, the reader is referred to the web version of this article.)

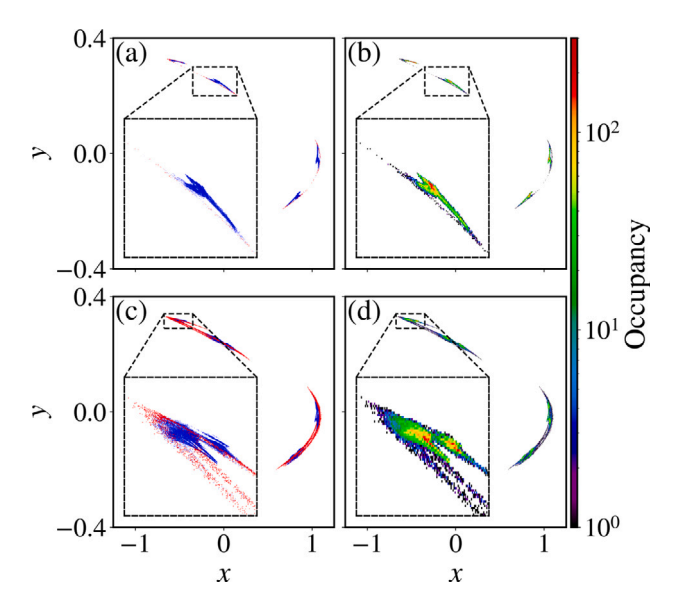


Fig. 8. (a) and (c) The phase space of the network and (b) and (d) the occupancy for $\sigma=0.174$ and r=0.25 with (top row) ascending order and (bottom row) descending order. We plot the x and y positions of each node after the transient and we color in blue (red) the coherent (incoherent) nodes and divide the phase space into a grid of 1000×1000 boxes and count the number of time each box was visited (occupancy). (For interpretation of the references to color in this figure legend, the reader is referred to the web version of this article.)

exhibits nondivergent dynamics. This counterintuitive behavior for the chosen parameter values is a consequence of the network coupling that stabilizes the divergent dynamics, being a collective phenomenon that could not be predicted only from the analysis of its composing parts.

Additionally, using an extended version of the spatial recurrence matrix, we have accurately characterized the dynamics of the network, where we have identified three distinct nondivergent states, namely, completely coherent and completely incoherent states and also coexisting coherent and incoherent nodes. We have found that for the same coupling strength and radius, different states coexist and have different spatial distributions in phase space. Moreover, by dividing the phase space into boxes and counting the number of times a box has been occupied along the time evolution of the network, we have found that regions with higher occupancy correspond to the location of the

coherent nodes. Although we focused on the dynamics of a discretetime network (mainly due to computational limitations), we strongly believe that our findings apply to continuous-time networks also, due to the similarities in the dynamics of both systems.

All the presented results were obtained for a network of N=1000 nodes, however, an interesting future work would be to identify a minimal network where an analytical approach could be feasible to determine the transition states.

CRediT authorship contribution statement

Vagner dos Santos: Writing – review & editing, Writing – original draft, Software, Formal analysis, Data curation, Conceptualization.

Matheus Rolim Sales: Writing – review & editing, Writing – original draft, Validation, Software, Methodology, Investigation, Formal analysis, Data curation, Conceptualization. Iberê Luiz Caldas: Writing – review & editing, Writing – original draft, Funding acquisition, Formal analysis, Conceptualization. Ricardo Luiz Viana: Writing – review & editing, Writing – original draft, Funding acquisition, Formal analysis, Conceptualization. José Danilo Szezech: Writing – review & editing, Writing – original draft, Investigation, Funding acquisition, Formal analysis, Conceptualization.

Declaration of competing interest

The authors declare that they have no known competing financial interests or personal relationships that could have appeared to influence the work reported in this paper.

Acknowledgments

We wish to acknowledge the support of the Araucária Foundation, Brazil, the Coordination of Superior Level Staff Improvement (CAPES), the National Council for Scientific and Technological Development (CNPq), Brazil under Grant No. 304616/2021-4, 309670/2023-3, 403120/2021-7 and 301019/2019-3, and the São Paulo Research Foundation (FAPESP), Brazil, under Grant No. 2018/03211-6, 2023/08698-9, and 2024/14825-6. We would also like to thank the 105 Group Science (www.105groupscience.com) for fruitful discussions.

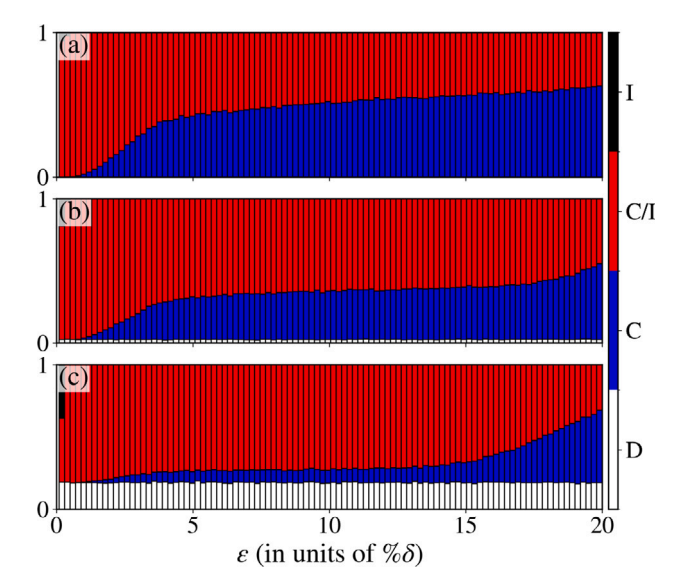


Fig. A.9. Fraction of initial conditions that converges to each state as a function of the threshold ϵ for the network (1) with N=1000 and r=0.25 for (a) $\sigma=0.30$, (b) $\sigma=0.32$, and (c) $\sigma=0.34$. The parameters used are $\alpha=1.5$, and $\beta=0.3$. The color code used is black for incoherent states (I), red for coherence–incoherence states (C/I), blue for coherent states (C), and white for divergent states (D). (For interpretation of the references to color in this figure legend, the reader is referred to the web version of this article.)

Appendix A. The effect of the threshold on the coherence/incoherence detection

In Section 3, we introduced the binary matrix L in terms of the distance matrix \mathbf{d} and the threshold ε [Eq. (3)]. We defined the threshold to be 7.5% of the standard deviation vector δ mean value. In order to analyze the effect of ε on the coherence/incoherence detection, we consider fixed values for the coupling radius (r=0.25), different coupling strength and choose 10^4 random initial conditions on the interval $[-0.1,0.1]\times[-0.1,0.1]$. We calculate the basin stability [55–57], i.e., the fraction of these initial conditions that converge to each of the four possible states, as a function of the threshold ε (Fig. A.9).

If the threshold is too small ($\varepsilon \sim 1\%\delta$), we detect almost no coherent states, and as ε grows larger, the number of coherent states grows as well, as expected. The rise is sharpest for large values of ε . However, there is an interval of values of ε in which the proportion of coherent and coherence–incoherence states does not change significantly ($\varepsilon \in [5\%\delta, 10\%\delta]$). Therefore, there is in fact a whole range of values of ε which yields good results.

Appendix B. Supplementary data

Supplementary material related to this article can be found online at https://doi.org/10.1016/j.chaos.2025.116115.

Data availability

The authors declare that the data supporting the findings of this study are available within the paper.

References

- [1] Strogatz SH. Exploring complex networks. Nature 2001;410(6825):268–76. http://dx.doi.org/10.1038/35065725.
- [2] Kaneko K. Theory and applications of coupled map lattices. Nonlinear Sci: Theory Appl 1993.

- [3] Anteneodo C, Batista A, Viana R. Chaos synchronization in long-range coupled map lattices. Phys Lett A 2004;326(3):227–33. http://dx.doi.org/ 10.1016/j.physleta.2004.04.035, https://www.sciencedirect.com/science/article/ pii/S0375960104005572.
- [4] Ren H-P, Bai C. Secure communication based on spatiotemporal chaos. Chin Phys B 2015;24(8):080503. http://dx.doi.org/10.1088/1674-1056/24/8/080503.
- [5] Hussain I, Gondal MA. An extended image encryption using chaotic coupled map and s-box transformation. Nonlinear Dynam 2014;76(2):1355–63. http: //dx.doi.org/10.1007/s11071-013-1214-z.
- [6] Lameu E, Batista C, Batista A, Iarosz K, Viana R, Lopes S, et al. Suppression of bursting synchronization in clustered scale-free (rich-club) neuronal networks. Chaos 2012;22(4). https://www.scopus.com/inward/record.uri?eid=2s2.0-84871907303&doi=10.1063%2f1.4772998&partnerID=40&md5= 52a70be3fd8beb5e655d9dda056c5c9a.
- [7] Batista CAS, Lameu EL, Batista AM, Lopes SR, Pereira T, Zamora-López G, et al. Phase synchronization of bursting neurons in clustered small-world networks. Phys Rev E 2012;86:016211. http://dx.doi.org/10.1103/PhysRevE.86.016211, https://link.aps.org/doi/10.1103/PhysRevE.86.016211.
- [8] Ferrari F, Viana R, Lopes S, Stoop R. Phase synchronization of coupled bursting neurons and the generalized Kuramoto model. Neural Netw 2015;66:107– 18. http://dx.doi.org/10.1016/j.neunet.2015.03.003, https://www.sciencedirect. com/science/article/pii/S0893608015000507.
- [9] Protachevicz PR, Borges FS, Lameu EL, Ji P, Iarosz KC, Kihara AH, et al. Bistable firing pattern in a neural network model. Front Comput Neurosci 2019;13. http://dx.doi.org/10.3389/fncom.2019.00019, https://www.frontiersin. org/journals/computational-neuroscience/articles/10.3389/fncom.2019.00019.
- [10] Zhang Y-Q, Wang X-Y. Spatiotemporal Chaos in mixed linear–nonlinear coupled logistic map lattice. Phys A 2014;402:104–18. http://dx.doi.org/10. 1016/j.physa.2014.01.051, https://www.sciencedirect.com/science/article/pii/ S0378437114000636.
- [11] Motter AE, Lai Y-C. Cascade-based attacks on complex networks. Phys Rev E 2002;66:065102. http://dx.doi.org/10.1103/PhysRevE.66.065102, https://link.aps.org/doi/10.1103/PhysRevE.66.065102.
- [12] Arenas A, Díaz-Guilera A, Kurths J, Moreno Y, Zhou C. Synchronization in complex networks. Phys Rep 2008;469(3):93–153. http://dx.doi.org/10. 1016/j.physrep.2008.09.002, https://www.sciencedirect.com/science/article/pii/ S0370157308003384.
- [13] Kuramoto Y, Battogtokh D. Coexistence of coherence and incoherence in nonlocally coupled phase oscillators. Nonlinear Phenom Complex Syst 2002;5:380.
- [14] Abrams DM, Strogatz SH. Chimera states for coupled oscillators. Phys Rev Lett 2004;93:174102. http://dx.doi.org/10.1103/PhysRevLett.93.174102, https://link.aps.org/doi/10.1103/PhysRevLett.93.174102.
- [15] Majhi S, Bera BK, Ghosh D, Perc M. Chimera states in neuronal networks: A review. Phys Life Rev 2019;28:100–21. http://dx.doi.org/10.1016/j.plrev.2018.09. 003, https://www.sciencedirect.com/science/article/pii/S1571064518301088.
- [16] Wang Z, Liu Z. A brief review of Chimera state in empirical brain networks. Front Physiol 2020;11:724. http://dx.doi.org/10.3389/fphys.2020.00724, https://www.frontiersin.org/journals/physiology/articles/10.3389/fphys.2020.00724.
- [17] Martens EA, Thutupalli S, Fourrière A, Hallatschek O. Chimera states in mechanical oscillator networks. Proc Natl Acad Sci 2013;110(26):10563-7. http://dx.doi.org/10.1073/pnas.1302880110, https://www.pnas.org/doi/abs/10.1073/pnas.1302880110.
- [18] Kapitaniak T, Kuzma P, Wojewoda J, Czolczynski K, Maistrenko Y. Imperfect Chimera states for coupled pendula. Sci Rep 2014;4(1):6379. http://dx.doi.org/ 10.1038/srep06379.
- [19] Nkomo S, Tinsley MR, Showalter K. Chimera states in populations of non-locally coupled chemical oscillators. Phys Rev Lett 2013;110:244102. http://dx.doi.org/10.1103/PhysRevLett.110.244102, https://link.aps.org/doi/10.1103/PhysRevLett.110.244102.
- [20] Totz JF, Rode J, Tinsley MR, Showalter K, Engel H. Spiral wave Chimera states in large populations of coupled chemical oscillators. Nat Phys 2018;14(3):282–5. http://dx.doi.org/10.1038/s41567-017-0005-8.
- [21] Lazarides N, Neofotistos G, Tsironis GP. Chimeras in squid metamaterials. Phys Rev B 2015;91:054303. http://dx.doi.org/10.1103/PhysRevB.91.054303, https://link.aps.org/doi/10.1103/PhysRevB.91.054303.
- [22] Hizanidis J, Lazarides N, Tsironis GP. Pattern formation and Chimera states in 2d squid metamaterials. Chaos: An Interdiscip J Nonlinear Sci 2020;30(1):013115. http://dx.doi.org/10.1063/1.5122307.
- [23] Rattenborg N, Amlaner C, Lima S. Behavioral, neurophysiological and evolutionary perspectives on unihemispheric sleep. Neurosci Biobehav Rev 2000;24(8):817–42. http://dx.doi.org/10.1016/S0149-7634(00)00039-7, https://www.sciencedirect.com/science/article/pii/S0149763400000397.
- [24] Glaze TA, Bahar S. Neural synchronization, Chimera states and sleep asymmetry. Front Netw Physiol 2021;1. http://dx.doi.org/10.3389/fnetp.2021.734332, https://www.frontiersin.org/journals/network-physiology/articles/10.3389/fnetp.2021.734332.
- [25] Andrzejak RG, Rummel C, Mormann F, Schindler K. All together now: Analogies between chimera state collapses and epileptic seizures. Sci Rep 2016;6(1):23000. http://dx.doi.org/10.1038/srep23000.

- [26] Medeiros ES, R. O. Medrano T, Caldas IL, Feudel U. Boundaries of synchronization in oscillator networks. Phys Rev E 2018;98:030201. http://dx.doi.org/10.1103/PhysRevE.98.030201, https://link.aps.org/doi/10.1103/PhysRevE.98.030201
- [27] Medeiros ES, R. O. Medrano T, Caldas IL, Feudel U. The impact of chaotic saddles on the synchronization of complex networks of discrete-time units. J Phys: Complexity 2021;2(3):035002. http://dx.doi.org/10.1088/2632-072X/abedc2.
- [28] Vasconcelos DB, Lopes SR, Viana RL, Kurths J. Spatial recurrence plots. Phys Rev E 2006;73:056207. http://dx.doi.org/10.1103/PhysRevE.73.056207, https://link.aps.org/doi/10.1103/PhysRevE.73.056207.
- [29] Santos MS, Szezech JD, Batista AM, Caldas IL, Viana RL, Lopes SR. Recurrence quantification analysis of Chimera states. Phys Lett A 2015;379(37):2188–92. http://dx.doi.org/10.1016/j.physleta.2015.07.029, https://www.sciencedirect.com/science/article/pii/S0375960115006313.
- [30] Nusse HE, Yorke JA. A procedure for finding numerical trajectories on chaotic saddles. Phys D: Nonlinear Phenom 1989;36(1):137–56. http: //dx.doi.org/10.1016/0167-2789(89)90253-4, https://www.sciencedirect.com/ science/article/pii/0167278989902534.
- [31] Wolfrum M, Omel'chenko OE. Chimera states are chaotic transients. Phys Rev E 2011;84:015201. http://dx.doi.org/10.1103/PhysRevE.84.015201, https://link. aps.org/doi/10.1103/PhysRevE.84.015201.
- [32] Pecora LM, Carroll TL. Master stability functions for synchronized coupled systems. Phys Rev Lett 1998;80:2109–12. http://dx.doi.org/10.1103/PhysRevLett. 80.2109, https://link.aps.org/doi/10.1103/PhysRevLett.80.2109.
- [33] Omelchenko I, Maistrenko Y, Hövel P, Schöll E. Loss of coherence in dynamical networks: Spatial chaos and Chimera states. Phys Rev Lett 2011;106:234102. http://dx.doi.org/10.1103/PhysRevLett.106.234102, https://link.aps.org/doi/10. 1103/PhysRevLett.106.234102.
- [34] Batista CAS, Viana RL. Quantifying coherence of Chimera states in coupled chaotic systems. Phys A 2019;526:120869. http://dx.doi.org/10.1016/j.physa.2019.04.105, https://www.sciencedirect.com/science/article/pii/S0378437119304790.
- [35] Batista CAS, da Silva ST, Viana RL. Characterization of Chimeras in coupled phase oscillators based on a coherence function. Commun Nonlinear Sci Numer Simul 2023;117:106921. http://dx.doi.org/10.1016/j.cnsns.2022.106921, https://www.sciencedirect.com/science/article/pii/S1007570422004087.
- [36] Gopal R, Chandrasekar VK, Venkatesan A, Lakshmanan M. Observation and characterization of Chimera states in coupled dynamical systems with nonlocal coupling. Phys Rev E 2014;89:052914. http://dx.doi.org/10.1103/PhysRevE.89. 052014
- [37] Ghosh S, Jalan S. Engineering Chimera patterns in networks using heterogeneous delays. Chaos: An Interdiscip J Nonlinear Sci 2018;28(7):071103. http://dx.doi. org/10.1063/1.5042133.
- [38] Kemeth FP, Haugland SW, Schmidt L, Kevrekidis IG, Krischer K. A classification scheme for Chimera states. Chaos: An Interdiscip J Nonlinear Sci 2016;26(9):094815. http://dx.doi.org/10.1063/1.4959804.
- [39] dos Santos V, Sales MR, Muni SS, Szezech JD, Batista AM, Yanchuk S, et al. Identification of single- and double-well coherence-incoherence patterns by the binary distance matrix. Commun Nonlinear Sci Numer Simul 2023;125:107390. http://dx.doi.org/10.1016/j.cnsns.2023.107390, https://www.sciencedirect.com/science/article/pii/S1007570423003088.
- [40] Parastesh F, Azarnoush H, Jafari S, Perc M. Detecting chimeras by eigenvalue decomposition of the bivariate local order parameter. Europhys Lett 2020;130(2):28003. http://dx.doi.org/10.1209/0295-5075/130/28003.
- [41] Eckmann J-P, Kamphorst SO, Ruelle D. Recurrence plots of dynamical systems. Europhys Lett 1987;4(9):973. http://dx.doi.org/10.1209/0295-5075/4/9/004.

- [42] Marwan N, Kurths J. Nonlinear analysis of bivariate data with cross recurrence plots. Phys Lett A 2002;302(5):299–307. http://dx.doi.org/10. 1016/S0375-9601(02)01170-2, https://www.sciencedirect.com/science/article/ pii/S0375960102011702.
- [43] Marwan N, Wessel N, Meyerfeldt U, Schirdewan A, Kurths J. Recurrence-plot-based measures of complexity and their application to heart-rate-variability data. Phys Rev E 2002;66:026702. http://dx.doi.org/10.1103/PhysRevE.66.026702, https://link.aps.org/doi/10.1103/PhysRevE.66.026702.
- [44] Marwan N, Carmen Romano M, Thiel M, Kurths J. Recurrence plots for the analysis of complex systems. Phys Rep 2007;438(5):237–329. http://dx.doi.org/ 10.1016/j.physrep.2006.11.001, https://www.sciencedirect.com/science/article/ pii/S0370157306004066.
- [45] Marwan N. A historical review of recurrence plots. Eur Phys J Special Top 2008;164(1):3–12. http://dx.doi.org/10.1140/epjst/e2008-00829-1.
- [46] Goswami B. A brief introduction to nonlinear time series analysis and recurrence plots. Vibration 2019;2(4):332–68. http://dx.doi.org/10.3390/vibration2040021, https://www.mdpi.com/2571-631X/2/4/21.
- [47] Mindlin GM, Gilmore R. Topological analysis and synthesis of chaotic time series. Phys D: Nonlinear Phenom 1992;58(1):229–42. http://dx.doi.org/10.1016/0167-2789(92)90111-Y, https://www.sciencedirect.com/science/article/pii/016727899290111Y.
- [48] Zbilut JP, Webber CL. Embeddings and delays as derived from quantification of recurrence plots. Phys Lett A 1992;171(3):199–203. http://dx.doi.org/10.1016/0375-9601(92)90426-M, https://www.sciencedirect.com/science/article/pii/037596019290426M.
- [49] Zbilut JP, Zaldivar-Comenges J-M, Strozzi F. Recurrence quantification based liapunov exponents for monitoring divergence in experimental data. Phys Lett A 2002;297(3):173–81. http://dx.doi.org/10.1016/S0375-9601(02)00436-X, https://www.sciencedirect.com/science/article/pii/S037596010200436X.
- [50] Thiel M, Romano M, Kurths J, Meucci R, Allaria E, Arecchi F. Influence of observational noise on the recurrence quantification analysis. Phys D: Nonlinear Phenom 2002;171(3):138–52. http://dx.doi.org/10.1016/S0167-2789(02)00586-9, https://www.sciencedirect.com/science/article/pii/S0167278902005869.
- [51] Sales MR, Mugnaine M, Szezech J, José D, Viana RL, Caldas IL, et al. Stickiness and recurrence plots: An entropy-based approach. Chaos: An Interdiscip J Nonlinear Sci 2023;33(3):033140. http://dx.doi.org/10.1063/5.0140613.
- [52] Souza LC, Sales MR, Mugnaine M, Szezech JD, Caldas IL, Viana RL. Chaotic escape of impurities and sticky orbits in toroidal plasmas. Phys Rev E 2024;109:015202. http://dx.doi.org/10.1103/PhysRevE.109.015202, https://link.aps.org/doi/10.1103/PhysRevE.109.015202.
- [53] Semenova N, Zakharova A, Schöll E, Anishchenko V. Does hyperbolicity impede emergence of chimera states in networks of nonlocally coupled chaotic oscillators? Europhys Lett 2015;112(4):40002. http://dx.doi.org/10.1209/0295-5075/112/40002.
- [54] Rybalova E, Semenova N, Strelkova G, Anishchenko V. Transition from complete synchronization to spatio-temporal chaos in coupled chaotic systems with nonhyperbolic and hyperbolic attractors. Eur Phys J Spec Top 2017;226(9):1857–66. http://dx.doi.org/10.1140/epjst/e2017-70023-1.
- [55] Menck PJ, Heitzig J, Marwan N, Kurths J. How basin stability complements the linear-stability paradigm. Nat Phys 2013;9(2):89–92. http://dx.doi.org/10.1038/ nphys2516.
- [56] Schultz P, Heitzig J, Kurths J. Detours around basin stability in power networks. New J Phys 2014;16(12):125001. http://dx.doi.org/10.1088/1367-2630/16/12/125001.
- [57] Rakshit S, Bera BK, Perc M, Ghosh D. Basin stability for Chimera states. Sci Rep 2017;7(1):2412. http://dx.doi.org/10.1038/s41598-017-02409-5.